

Chapter 6

Optical bistability in coupled micro-cavities

6.1 Introduction

The details of \mathcal{PT} –symmetric system have been discussed in previous chapter. In this chapter we illustrate the possible applications of \mathcal{PT} –symmetric system via optical bistability (OB) and higher order sideband generation (HSG). The \mathcal{PT} –symmetric systems are generally characterized by non-Hermitian Hamiltonians. The non-Hermitian Hamiltonian of a system supplies the lifetimes as well as energies of the states. The \mathcal{PT} –symmetric system with loss and gain, is basically an open quantum system (OQS). The OQSs are explained via projection operator approach [187]. These systems are enclosed by an environment. So, there is a possibility of an external mixing of the states via scattering wavefunctions with common environment. The existence of the phase transition point i.e. exceptional point (EP) for a \mathcal{PT} –symmetry system is mathematically interpreted via external mixing. The lifetimes of the two adjacent eigenstates divide or bifurcate due to effect of EP [188-190]. In the dynamics of OQSs (with two or more eigenstates) another interesting occurrence is possible, known as dynamical phase transition (DPT). This is related to clustering of EPs. DPT has been already theoretically illustrated and experimentally verified [191-199]. It has been also reported that different spectroscopic factors are altered reasonably with respect to some adjustable parameters [187, 200]. The model studied here a \mathcal{PT} –symmetric system and there is a possibility of phase transition. In this chapter we focused to the phase transition effect on bistability.

Optical bistability and optical multistability are non-linear optical effects. These effects have already been studied in different optical systems such as atom-assisted cavities [201], ring cavity [202], micro-resonator OMS [203], OMS with B-E condensate [204],

cavity polariton OMS [205] etc. These have useful applications in memory storage, sensitive force detection, optical transistor and optical switch [206-213].

In ref. [214] Liu et al studied bistability effect with the system of nonlinear periodic \mathcal{PT} –symmetric potential. Minh et al [215] illustrated OB in a gaseous medium with giant Kerr-nonlinearity. Bass et al [216] experimentally demonstrated polariton bistability in semiconductor cavity via polaritonic Kerr effect. So, Kerr nonlinear optical medium take part a vital role for various optical effects. The present system of our study consists of two coupled micro-cavities. One cavity has Kerr medium.

Here we have also addressed power spectrum of the output field. Power spectrum implies arrangements of power into different frequencies. The analysis of power spectrum can be done by discrete Fourier transform, exponential series simulation, fast Fourier transform (FFT) etc. Here, we have studied variation of steady state correlation function numerically by using FFT. HSG in different optical system has been reported in various studies such as OMS containing photonic molecule [217], two-cavity system with modulated coupling [218] etc. In our study, we have analyzed the possibility of HSG in two micro-cavity system and also discussed the effect of Kerr strength and tunnelling strength on it.

6.2 Physical system

The model system is considered here to study optical bistability and higher order sideband generation, already has discussed in section 5.3. Here, the passive and active cavity field modes are characterized by field operator a and b , respectively. The model system is depicted in figure 6.1. The system Hamiltonian is written as

$$H_s = \left(\omega_a - \frac{ik_a}{2} \right) a^\dagger a + \left(\omega_b - \frac{ik_b}{2} \right) b^\dagger b + J(ab^\dagger + h.c.) + Ua^{\dagger 2}a^2 + (\Omega_d a^\dagger e^{-i\omega_a t} + h.c.) \quad (6.1)$$

The passive and active cavity resonance frequencies are ω_a and ω_b . Other terms are same as in section 5.3 of chapter 5.

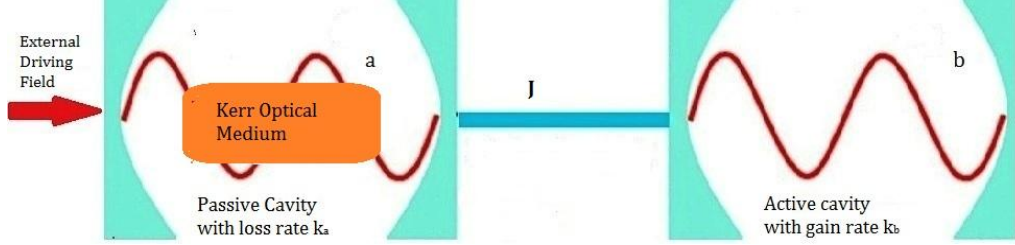


Figure 6.1: Schematic diagram of the PT-symmetric coupled micro-cavities

6.3 Steady state solution

The Hamiltonian of equation (6.1) is transformed by means of the operator $\mathcal{U}(t) = \exp\{-i\omega_d(a^\dagger a + b^\dagger b)t\}$ and using equation $H' = \mathcal{U}^\dagger(t) H \mathcal{U}(t) - i \mathcal{U}^\dagger(t) \frac{\partial \mathcal{U}(t)}{\partial t}$. We obtain the transformed Hamiltonian as follows:

$$H' = \Delta_a a^\dagger a + \Delta_b b^\dagger b + J(a^\dagger b + ab^\dagger) + U a^{\dagger 2} a^2 + \Omega_d (a^\dagger + a) \quad (6.2)$$

Where $\Delta_a = \omega_a - \omega_d$ and $\Delta_b = \omega_b - \omega_d$ represent the frequency detuning between passive and active cavity field mode (a, b) and the external driving field. The quantum HLEs for the passive and active field modes are given by

$$\begin{aligned} \dot{a} &= -\left(i\Delta_a + \frac{k_a}{2}\right)a - iJb - 2iUa^\dagger a^2 - i\Omega_d + \sqrt{2k_a}a^{in} \\ \dot{b} &= -\left(i\Delta_b + \frac{k_b}{2}\right)b - iJa + \sqrt{2k_b}b^{in} \end{aligned} \quad (6.3)$$

The noise operators a^{in} and b^{in} of passive and active field modes satisfy following relations

$$\begin{aligned} \langle a^{in}(t)a^{\dagger in}(t') \rangle &= \langle b^{in}(t)b^{\dagger in}(t') \rangle = \delta(t - t') \\ \langle a^{\dagger in}(t)a^{in}(t') \rangle &= \langle b^{\dagger in}(t)b^{in}(t') \rangle = 0 \end{aligned} \quad (6.4)$$

The average values of the noise operators are zero, for Markovian consideration. In presence of strong input laser field, any field operator can be expressed as sum of steady state values and quantum fluctuation. So, the passive and active field operators

take the form $a \rightarrow \alpha_1 + \delta a$ and $b \rightarrow \beta_1 + \delta b$, where α_1 , β_1 are steady values of the field modes and δa , δb are small fluctuations. The steady values of the cavity field modes satisfy semi-classical equation as

$$\begin{aligned}\dot{\alpha}_1 &= -\left(i\Delta_a + \frac{k_a}{2}\right)\alpha_1 - iJ\beta_1 - 2iU|\alpha_1|^2\alpha_1 - i\Omega_d \\ \dot{\beta}_1 &= -\left(i\Delta_b + \frac{k_b}{2}\right)\beta_1 - iJ\alpha_1\end{aligned}\quad (6.5)$$

The steady state solutions for passive and active cavity field modes are obtained as

$$\begin{aligned}\alpha_1 &= -\frac{i\Omega_d}{\left(i\Delta_a + \frac{k_a}{2}\right) + \frac{J^2}{\left(i\Delta_b + \frac{k_b}{2}\right)} + 2iU|\alpha_1|^2} \\ \beta_1 &= -\frac{iJ\alpha_1}{\left(i\Delta_b + \frac{k_b}{2}\right)}\end{aligned}\quad (6.6)$$

For very weak Kerr nonlinear strength $U \sim 0$, we obtain the following expression for mean passive cavity photon number

$$|\alpha_1|^2 = \frac{2\Omega_d^2\Delta_b'^2}{2\Delta_a'^2\Delta_b'^2 + 2J^4 + J^2(k_a k_b - 4\Delta_a\Delta_b)}\quad (6.7)$$

Where $\Delta_a'^2 = \Delta_a^2 + \frac{k_a^2}{4}$ and $\Delta_b'^2 = \Delta_b^2 + \frac{k_b^2}{4}$

6.4 Optical Bistability

To illustrate the optical bistability in present system, we have analyzed the mathematical expression of α_1 from equation (6.6) and discussed how the OB can be controlled via different system parameters. Simplifying equation (6.6), we obtain the following expression of $|\alpha_1|^2$.

$$\begin{aligned}4|\alpha_1|^6 U^2 + \frac{4}{\Delta_b'^2} |\alpha_1|^4 U (\Delta_a \Delta_b'^2 - J^2 \Delta_b) \\ + \frac{1}{2\Delta_b'^2} |\alpha_1|^2 [2\Delta_a'^2 \Delta_b'^2 + J^2 (k_a k_b - 4\Delta_a \Delta_b) + 2J^4] = \Omega_d^2\end{aligned}\quad (6.8)$$

The above equation (6.8) is a cubic equation of mean passive cavity photon number (MPCPN) $|\alpha_1|^2$. So, it has three roots.

For optical bistability the condition is $\frac{\partial \Omega_d^2}{\partial |\alpha_1|^2} = 0$. Using this, we obtain

$$12|\alpha_1|^4 U^2 + \frac{8}{\Delta_b^2} |\alpha_1|^2 U (\Delta_a \Delta_b'^2 - J^2 \Delta_b) + \frac{1}{2\Delta_b^2} [2\Delta_a'^2 \Delta_b'^2 + J^2 (k_a k_b - 4\Delta_a \Delta_b) + 2J^4] = 0 \quad (6.9)$$

The above equation (6.9) is a quadratic equation of $|\alpha_1|^2$. It has two different roots if the discriminant is positive. This yield

$$\frac{U^2}{\Delta_b^2} \left[8(\Delta_a \Delta_b'^2 - J^2 \Delta_b)^2 + 3\{2\Delta_a'^2 \Delta_b'^2 + J^2 (k_a k_b - 4\Delta_a \Delta_b) + 2J^4\} \right] > 0 \quad (6.10)$$

The variation of MPCPN is depicted in figure 6.2 (a-f), as a function of normalised driving strength for different Kerr nonlinear strength, photon tunnelling strength. Figure 6.2 (a-d) display the variation for $J/k_a = 0$, $J/k_a = 0.3$, $J/k_a = 0.5$ and $J/k_a = 0.7$, respectively. The graphical representation is S -shaped nature. This implies the presence of bistable states in the system. Among the three roots of the equation (6.8), the largest and smallest roots are stable. The middle root is unstable. Alternatively, the variation of $|\alpha_1|^2$ may also be interpreted as hysteresis. If we increase the external driving strength or input power continuously from zero, $|\alpha_1|^2$ remains in lower stable state up-to $\Omega_d/k_a \sim 1$. If we further increase input power the MPCPN jumps from smaller to larger value i.e. lower stable state to upper stable state (shown by arrow lines in figure 6.2c). For driving strength $\Omega_d/k_a > 1$ the state remains in upper stable branch. If we decrease the input power, hence driving strength, $|\alpha_1|^2$ returns back to the initial point of the upper stable state. When driving strength further decreases $|\alpha_1|^2$ return back to lower state (arrow line indicates the transition in figure 6.2c).

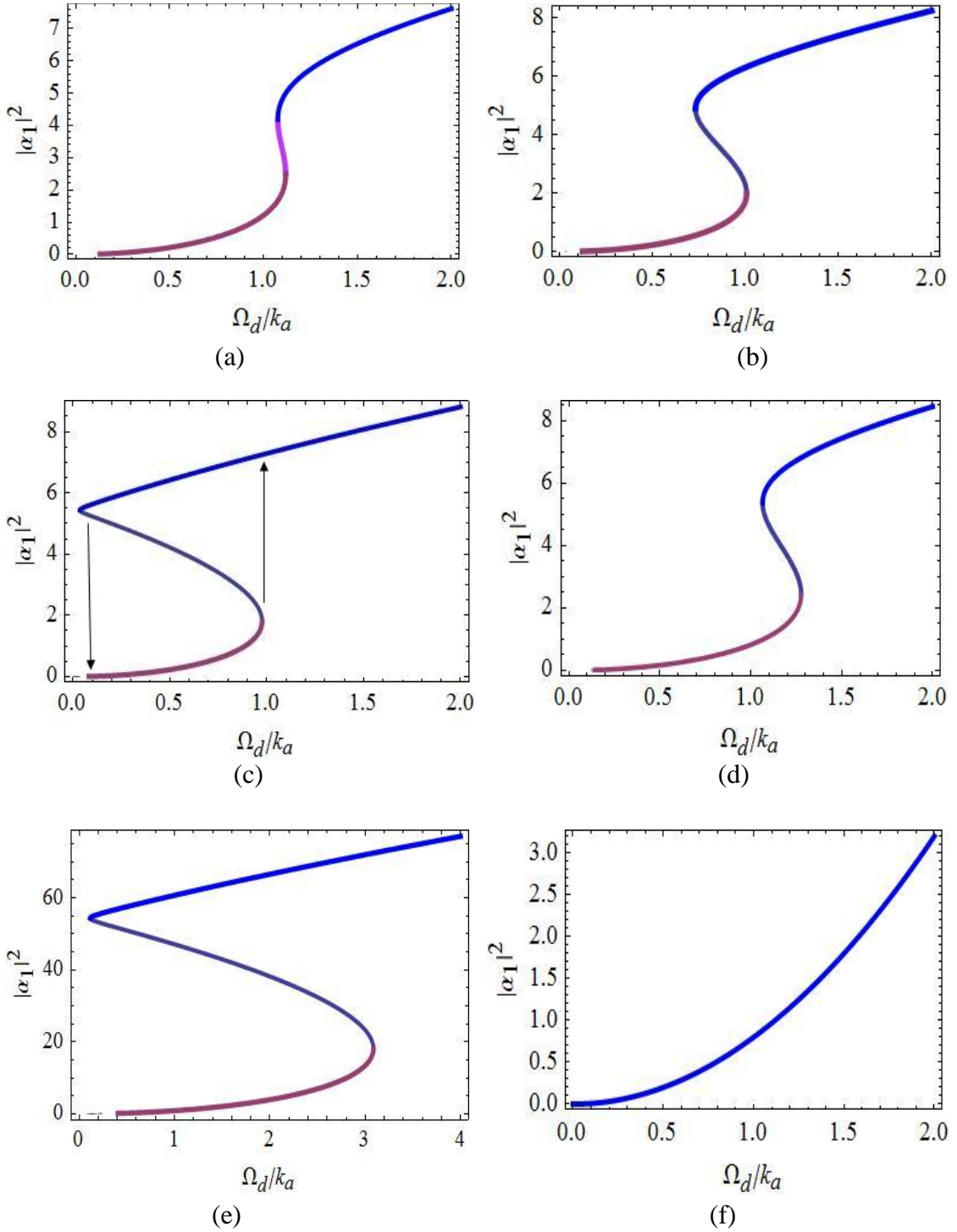


Figure 6.2: Mean cavity photon number as a function of normalised driving strength with different values of mode coupling strength and Kerr-nonlinearity strength (a) $J/k_a = 0$ and $U/k_a = 0.1$ (b) $J/k_a = 0.3$ and $U/k_a = 0.1$ (c) $J/k_a = 0.5$, $U/k_a = 0.1$ (d) $J/k_a = 0.7$, $U/k_a = 0.1$ (e) $J/k_a = 0.5$, $U/k_a = 0.01$ (f) $J/k_a = 0.5$, $U/k_a = 0$; The other parameters are $k_b/k_a = -1$, $\Delta_a/k_a = -1$ and $\Delta_b/k_a = 0.09$.

Interestingly, the stability of the states is controlled by photon tunnelling strength i.e. adjusting separation between the two micro-cavities. The separation between the states lengthened due to position dependent phase shift of the optical field mode. The bistability effect is prominent at exceptional point (EP), which is clear from figure 6.2c. The phase rigidity of the wavefunctions reaches its optimum value at EP and hence the system exhibit effective bistability. Again, this is also illustrated by optimum width bifurcation i.e. the lifetimes of the nearby eigenstates bifurcated under the impact of EP. Figure 6.2e display the same variation at EP with lower value of Kerr nonlinear strength $U/k_a = 0.01$. It is observed that bistability effect is possible for larger driving strength. For very weak nonlinear strength $U/k_a \approx 0$, the bistability is ruled out, as depicted in figure 6.2f. So, it is argued that the Kerr nonlinearity plays the important role for optical bistability and one can manipulate threshold intensity by changing nonlinear strength, placed in passive cavity. Again, the hysteresis of MPCPN is tuned via controlling the photon tunnelling strength between the cavities.

6.4 Possibility of all-optical-switching

In this section, the possibility of efficient all-optical switching effect of the cavity photon number is discussed in present system. Here, it is considered that both the cavities have same frequency detuning i.e. $\Delta_a = \Delta_b = \Delta$. The variation of MPCPN is displayed as a function of frequency detuning in figure 6.3(a-d). Figure 6.3 (a-b) represent the variation for very weak nonlinearity. In figure 6.3a, we depict how the MPCPN explicitly depends on the cavity detuning for different values of gain-to-loss ratio (PPCS and PACS). It is clear that split resonance profiles of $|\alpha_1|^2$ is symmetric around normalised zero cavity detuning. The sharpness nature of the profiles around $\Delta/k_a = 0$, shows that the present system may be useful for designing efficient

all-optical switch. The sharpness nature is more effective for PACS. So, one can control the sharpness of switching by controlling the ratio of k_b/k_a . Figure 6.3(b) depicts the switching for wide zero intensity window. The wideness of the zero intensity window is adjusted by tuning the tunnelling strength between the cavities.

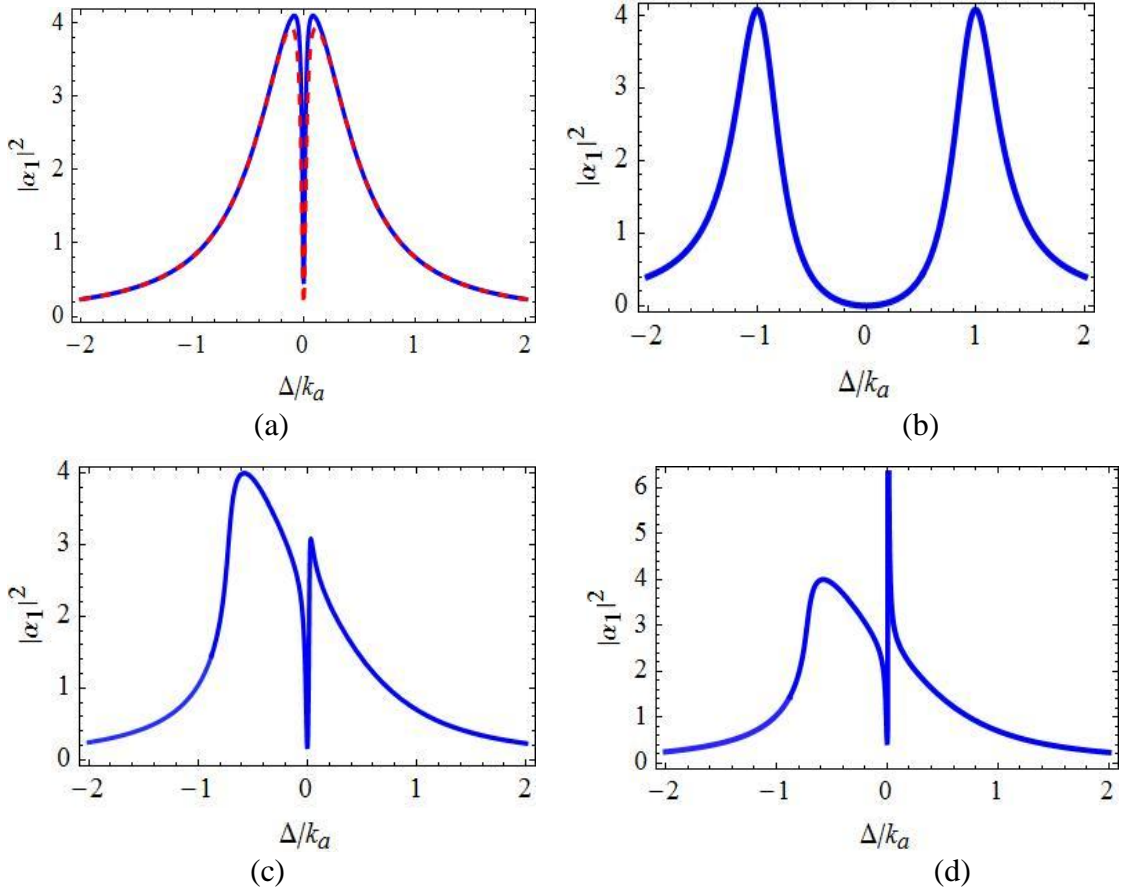


Figure 6.3: Mean cavity photon number as a function of normalised cavity detuning with different gain-to-loss ratio and mode coupling strength (a) $k_b/k_a = 0.01$ (dashed red), $k_b/k_a = -0.01$ (solid blue), $J/k_a = 0.1$ and (b) $k_b/k_a = 0.01$, $J/k_a = 1$ (c) $k_b/k_a = 0.01$, $J/k_a = 0.1$, $U/k_a = 0.1$ and (d) $k_b/k_a = -0.01$, $J/k_a = 1$, $U/k_a = 0.1$. The normalised driving strength is $\Omega_d/k_a = 1$.

Figure 6.3 (c) and (d) show the variation with considerable Kerr nonlinear strength for PPCS and PACS, respectively. To obtain the result in presence of considerable nonlinear term, we solve the expression of α_1 from equation (6.6). Here, the split resonance profile is asymmetric around zero frequency detuning. The sharpness and

intensity of the resonance profile is more prominent for PACS. For larger value of photon tunnelling strength the nature is almost symmetric and with tunable zero intensity window, similar variation occurs like figure 6.3 b. So, switching of the MPCPN may enable and disable via tuning the parameters of the input field, nonlinear strength, tunnelling strength and gain-to-loss ratio.

6.5 Optical Memory

Optical bistability effect of the present system has already been illustrated in previous section 6.4. So, it is clear that the MPCPN exhibits two stable states and these are tunable i.e. it leads to controlled optical bistability. This property may be useful as an optical memory element, like optical flip-flop.

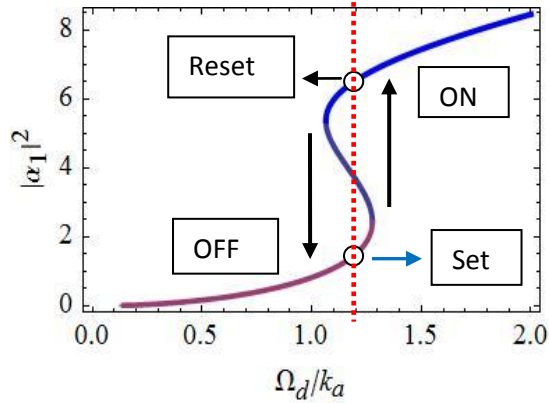


Figure 6.4: Plot of mean cavity photon number as a function of normalised driving strength with $J/k_a = 0.7$, $U/k_a = 0.1$, $\Delta_a/k_a = -1$, $k_b/k_a = -1$ and $\Delta_b/k_a = 0.09$.

Figure 6.4 shows the variation of $|\alpha_1|^2$ with respect to normalised driving strength. Here, we set the driving strength $\Omega_d/k_a \sim 1.2$ as biasing strength. When $\Omega_d/k_a > 1.2$ the MPCPN goes from lower stable state to upper stable state, the system is in ON state, just like the SET condition of a flip-flop. Again, $\Omega_d/k_a < 1.2$ the MPCPN jumps from upper state to lower state i.e. the system is in OFF state, like RESET. So, the present system may be useful as an optical flip-flop, which will be compact in size and

faster than traditional electronic flip-flop. One can tune the biasing driving strength through controlling photon tunnelling rate.

6.7 Power spectrum

Here, we have illustrated the power spectrum by using FFT. The spreading of power into different frequency components can be calculated by the correlation function

$$S(\omega) = \int_{-\infty}^{\infty} \langle a(\tau)b(0) \rangle e^{-i\omega\tau} d\tau, \text{ where } \omega \text{ indicates the spectrometric frequency.}$$

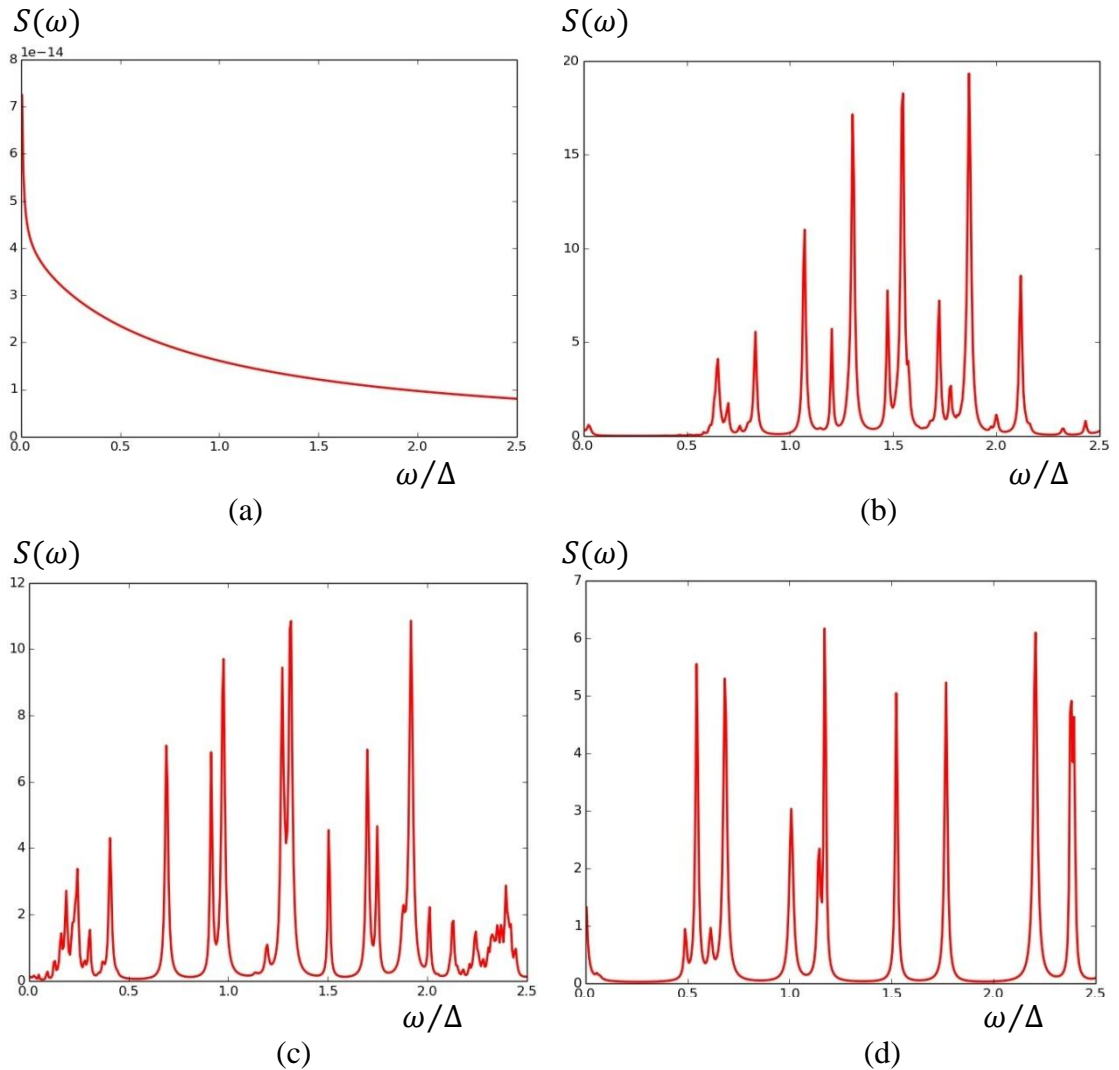


Figure 6.5: Variation of $S(\omega)$ as a function of normalized frequency ω/Δ with different mode coupling strength a) $J = 0$ b) $J = 2\pi \times 0.5 \times 5.35 \text{ MHz}$ c) $J = 2\pi \times 1.0 \times 5.35 \text{ MHz}$ d) $J = 2\pi \times 2.5 \times 5.35 \text{ MHz}$. The other parameters are $U/\Delta = 1.07$, $\Omega/\Delta = 0.107$, $\Delta = 2\pi \times 1 \text{ MHz}$ and $k_2/k_1 = 1$.

The variation of spectral power as a function of normalised frequency for various photon tunnelling rate and nonlinear strength is displayed in figure 6.5 and 6.6. To illustrate the influence of the photon tunnelling rate on sideband generation, we depict $S(\omega)$ vs rescaled frequency ω/Δ in figure 6.5 (a-d). It is clear that no sideband generation is possible for zero photon tunneling (Figure 6.5 a). For non-zero photon tunneling rate sideband generation is possible (Figure 6.5(b-d)). The number of sideband increases as tunneling rate increases. Again, number of sideband increases the spectral power decreases. So, one can tune the number of higher order sideband via adjusting photon tunneling rate between the cavities. Interestingly, the frequency spacing is more or less equal and almost with same power for higher tunneling rate as shown in figure 6.5(d). Figure 6.6 (a-b) shows the same variation for lower nonlinear strength. It can be stated that here spectral power decreases as nonlinearity decreases but number of sideband increases. Here, spectral distribution of positive frequencies is shown but it is possible to generate both positive and negative frequency domain as per FFT.

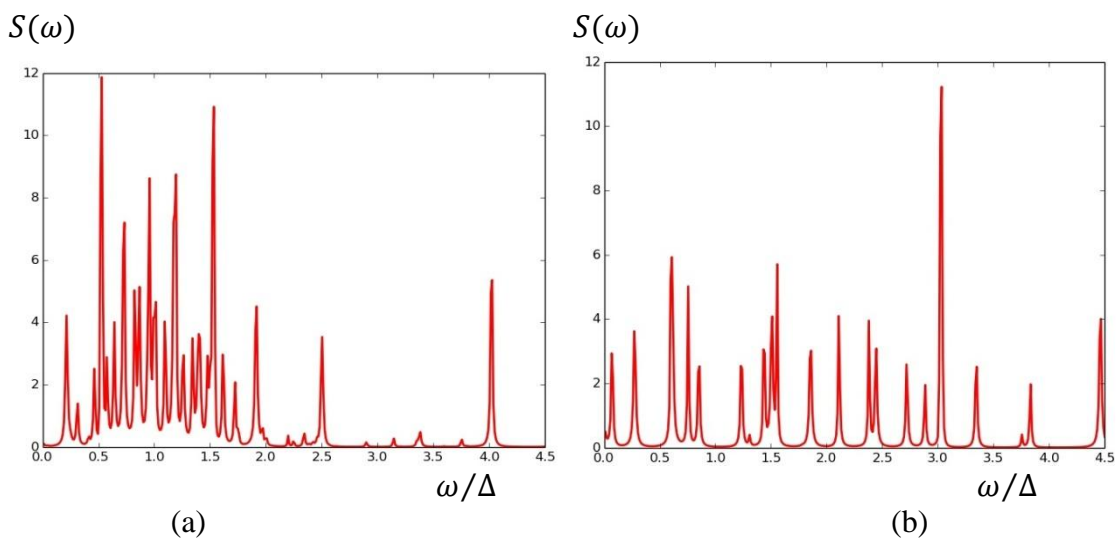


Figure 6.6: Variation of $S(\omega)$ as a function of normalized frequency ω/Δ with different mode coupling strength a) $J = 2\pi \times 0.5 \times 5.35 \text{ MHz}$ b) $J = 2\pi \times 2.0 \times 5.35 \text{ MHz}$. The other parameters are $U/\Delta = 1.07$, $\Omega/\Delta = 0.107$, $\Delta = 2\pi \times 1 \text{ MHz}$ and $k_2/k_1 = 1$.

6.8 Summary

In the present study, we have discussed OB and HSG in PT-symmetric coupled micro-cavities. The controllability of bistable nature via different system parameters has been reported.

To study bistable effect, the MPCPN is calculated by using Heisenberg-Langevin EOM for different field modes. The MPCPN has three roots for an applied driving strength, which is obtained via steady state solution. The largest and smallest roots are steady but middle one is changeable, this gives the signature of bistability in the present system. The variation of MPCPN can be illustrated as hysteresis. At EP, bistable effect is prominent due to width bifurcation i.e. lifetimes of the eigenstates are affected by EP. Alternatively, at EP, phase rigidity of the wavefunctions is optimum. As the system reveals two stable states, it behaves like flip-flop. This characteristic is practical for scheming of an optical memory element.

The variation of MPCPN (as a function of rescaled cavity detuning) shows symmetric split resonance profiles around zero frequency detuning for very weak Kerr nonlinear strength. The profile is asymmetric for considerable nonlinearity. The zero intensity window of MPCPN can be controlled through adjusting tunnelling rate. The preciseness of switching of MPCPN is more pronounced for PACS as compared to PPCS. So, switching can be tuned by adjusting gain-to-loss ratio i.e. adjusting interaction between environment and the system. This result might be advantageous to design optical sensor or sensitive all optical-switch.

Again, the present system consists of a passive nonlinear cavity coupled to an active cavity. So, controlled bistability can also be obtained by placing different Kerr medium

in passive cavity. From the study, it is clear that for lower Kerr nonlinearity, bistability can be achieved for higher input power. So, using higher nonlinear strength Kerr material in passive cavity one can reduce threshold power, which may be suitable for an optical power limiter.

The power spectrum is studied using FFT. The number of sideband can be tuned via adjusting photon tunnelling rate between the micro-cavities. For zero tunnelling there is no possibility of sideband generation. The spectral power may be controlled by inserting different Kerr medium in passive micro-cavity.